Earth Planet. Sci. Lett. 674 (2026) 119762

Contents lists available at ScienceDirect

Earth and Planetary Science Letters

journal homepage: www.elsevier.com/locate/epsl

The role of thermo-poro-elastic effects in the interpretation of gravity data

Massimo Nespoli *, Maurizio Bonafede, Maria Elina Belardinelli

Alma Mater Studiorum, University of Bologna, Department of Physics and Astronomy "Augusto Righi", Viale Berti Pichat 8, Bologna 40127, Italy

ARTICLE INFO

Edited by: Dr C. M. Petrone

Dataset link: https://doi.org/10.5281/zenodo.15101527

Keywords:
Volcanic gases
Gravity
Inclusion
TPE
Thermo-Poro-Elasticity
Hydrothermal systems

ABSTRACT

The study of gravity changes induced by magma chambers in volcanic environments has long been used to monitor unrest phases and to estimate the volumes and masses of magma intrusions. However, magma is not the sole driver of the observed deformation and gravity changes. Hydrothermal systems within the volcanic structure can also play a significant role. Recent advances in Thermo-Poro-Elastic (TPE) inclusion models have made it possible to efficiently and accurately simulate the mechanical effects caused by an increase of temperature and pore-pressure of fluids in a reservoir. In this work, we calculate the gravity variations induced by a disk-shaped inclusion. We model gravity variations induced by increments of pore-pressure and temperature within different fluid phases. We also consider the superposition of the effects of a TPE inclusion with a deeper magma chamber. The comparison with the data measured at the Campi Flegrei caldera (Italy) allows us to draw some suggestions on the use and interpretation of these results. Our findings demonstrate that these effects are significant and cannot be overlooked when interpreting gravimetric data during unrest phases and to assess geohazard levels.

1. Introduction

Interpreting different data is extremely important to understand unrest phases in volcanic areas. In addition to magmatic eruptions, phreatic eruptions, caused by sudden steam expansion, are highly dangerous (Gottsmann et al., 2019; Narita et al., 2020). The geophysical observables that are most promising for studying unrest phases are ground deformation, seismic, and gravimetric data. Today, ground deformation can be measured with submillimetric precision and high spatial and temporal resolution thanks to geodetic data from GNSS (Global Navigation Satellite System) stations and InSAR (Interferometric Synthetic Aperture Radar) satellites (e.g. Polcari et al., 2022). These data allow estimating with excellent precision the location, the dimension and the "potency" (i.e., a measure of its ability to deform the surrounding medium) of a possible source that may be responsible for the observed ground deformation. Inversion methods of geodetic data are generally based on preliminary assumptions, such as the type of deformation sources (e.g. Segall, 2010; Bonafede et al., 2022). The latter can be modeled using dislocations (Okada, 1985), cracks, and pressurized sources with various shapes (Yang et al., 1988; Mogi, 1958; Davis, 1986), which represent features such as dikes and magmatic intrusions. Alternatively, Thermo-Poro-Elastic (TPE) inclusions (Belardinelli et al., 2022; Mantiloni et al., 2020; Currenti et al., 2024) can simulate the effects of hot, pressurized hydrothermal fluids permeating a volume within the crust. A possible scenario in which a TPE inclusion is placed above a magma chamber is sketched in Fig. 1: a plume of hot, pressurized fluids released from a deep magma reservoir moves through a brittle layer separating the shallow meteoric aquifer (which can have high levels of gas saturation) from the deeper system (e.g. Zencher et al., 2006; Nespoli et al., 2025). During periods of unrest, stress from the magmatic reservoir can fracture part of this brittle layer, increasing its permeability. Fracturing enables fluids from the deep system to rise into the shallow meteoric aquifer enhancing seismicity due to the increasing pore-pressure. The deformation and seismic activity accompanying the emplacement of hot and pressurized fluids within the fractured brittle zone can be described using a TPE inclusion model. TPE models were recently applied to study the unrest phases of the Campi Flegrei caldera, Italy (Nespoli et al., 2021, 2023b) and the island of Vulcano, Italy (Stissi et al., 2023).

The same geodetic dataset can lend to multiple interpretations (e.g. Bonafede et al., 2022) which, do not allow for an univocal vision. For this reason, it is important to also consider seismic data. The location, magnitude and type of earthquakes, together with seismic tomography, can provide important information on the state of stress at depth which in turn can reveal the type and location of deep structures and buried deformation sources (e.g. D'Auria et al., 2014; Belardinelli et al., 2019; Nespoli et al., 2023b; Calò and Tramelli, 2018; De Siena et al., 2010).

In addition to geodetic and seismic data, gravimetric measurements

* Corresponding author.
E-mail address: massimo.nespoli2@unibo.it (M. Nespoli).

https://doi.org/10.1016/j.epsl.2025.119762
Received 5 April 2025; Received in revised form 14 November 2025; Accepted 22 November 2025

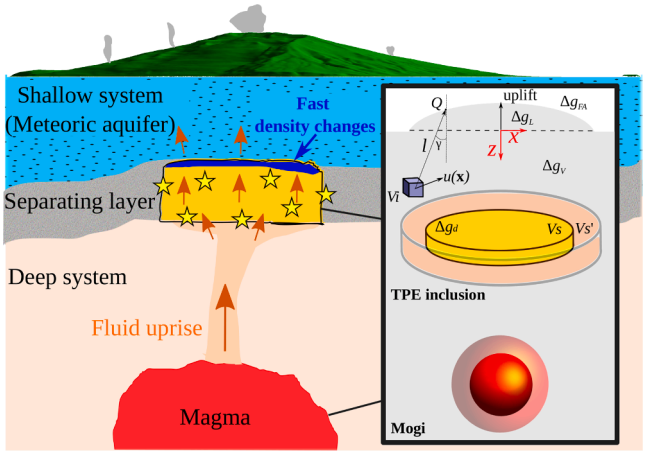

Fig. 1. Sketch a possible scenario in which a TPE inclusion (orange) is located above a deeper magma chamber (red) in a volcanic system. The exsolved fluids (arrows) released from the magma chamber rise toward a brittle layer (gray) separating the deep circulation from the shallower (meteoric aquifer in light blue) one. The fractured, permeable part of the layer can be represented by a TPE inclusion that acts as a deformation source and it is able to generate seismicity. In the inset the reference system is shown which is employed in the following computations, assuming a disk-shaped TPE inclusion and a spherical magma chamber (Mogi's). Q represents the location of a benchmark.

provide gravity variations with an accuracy of a few μGal (Berrino and Ricciardi, 2020), and modern absolute gravimeters are also capable of capturing sub-hourly variations. Measurements of time-space variations in the gravity field provide a powerful tool for detecting subsurface mass changes and redistributions (e.g. Battaglia et al., 2003; Calahorrano-Di Patre et al., 2019). These changes can result from density variations caused by the deformation induced by a source or from the addition (or loss) of mass in the volcano system (e.g. Sasai, 1986). Since gravimetric data allow us to estimate the magnitude of mass input/output involved, they are very important for predicting the size of a possible eruption and in distinguishing the magmatic contribution from the hydrothermal one. However, their interpretation remains challenging, as the same gravity variation can have multiple causes and the inversions of gravity and deformation data can yield sources of different natures: magmatic, hybrid, or purely hydrothermal (e.g. Battaglia et al., 2006, Gottssmann et al. 2006, Miller at al., 2018). For this reason, it is crucial to further develop and refine physical models.

To model the gravity variations induced by deformation sources in a laterally heterogeneous medium, numerical methods can be used (e.g. Trasatti and Bonafede, 2008; Currenti et al., 2007; Todesco and Berrino, 2005). Analytical approaches were also used to study gravity changes induced by magma (Walsh and Rice, 1979; Wong and Walsh, 1991; Fernández and Rundle, 1994; Bonafede and Mazzanti, 1999; Nikkhoo and Rivalta, 2022), even considering visco-elastic effects (Bonafede and Ferrari, 2009). While various literature has been written on the gravity variations induced by magma-filled deformation sources, in this work we show how important it is considering also the gravimetric effects induced by TPE inclusions which simultaneously, rapidly and accurately explain geodetic, seismic and gravimetric data.

2. Methodology

2.1. Mechanical effects of a TPE inclusion

Following Eshelby (1957), TPE inclusions represent confined rock volumes experiencing changes in pore pressure, Δp and temperature, ΔT embedded within a poro-elastic medium under drained and isothermal conditions (Belardinelli et al., 2019; Nespoli et al., 2025). The strain e_{ij} induced by a TPE inclusion can be computed as (Belardinelli et al., 2019; McTigue, 1986):

$$e_{ij} = \frac{1}{2\mu}\left(\tau_{ij} - \frac{\nu}{1+\nu}\tau_{kk}\delta_{ij}\right) + e_0\delta_{ij} \tag{1}$$

where μ is the rigidity, τ_{ij} is the stress, ν is the Poisson's ratio and e_0 is TPE inclusion potency. The latter is defined as:

$$e_0 = \frac{1}{3H}\Delta p + \frac{1}{3}\alpha_s \Delta T \tag{2}$$

where α_s is the thermal expansion of the solid phase and H is the poroelastic parameter (Biot, 1941). The latter can be expressed in terms of the drained incompressibility of the poro-elastic medium, K and that of the solid phase K_S' (as is often assumed), through the relation $1/H = 1/K - 1/K_S'$. The quantity e_0 is termed "potency" as it determines the magnitude of displacement, strain, and stress fields generated by the TPE inclusion. The displacement, u_i is computed by an integration over the volume V_s of the inclusion:

$$u_i(\mathbf{x}) = 3Ke_0 \int_{V_s} \frac{\partial G_{ik}}{\partial y_k}(\mathbf{x}, \mathbf{y}) dV_s \tag{3}$$

where G_{ik} is the Green's tensor for a half-space in isothermal and drained conditions. It indicates the displacement in the i th direction at $\mathbf{x}$ due to a unitary force acting in the k-th direction located at $\mathbf{y}$. The stress inside the source can be computed as:

$$\tau_{ij} = \lambda e_{kk}\delta_{ij} + 2\mu e_{ij} - 3Ke_0\delta_{ij} \tag{4}$$

while outside the inclusion it can be computed as:

$$\tau_{ij} = \lambda e_{kk}\delta_{ij} + 2\mu e_{ij} \tag{5}$$

In last years analytical solutions were proposed to compute such solutions in a full-space for a spherical shell TPE (Belardinelli et al., 2019) and thin disks (Belardinelli et al., 2022). Semi-analytical approaches to model thin disks in an half-space were proposed by Mantiloni et al. (2020). More recently Nespoli et al. (2021) and Benussi et al. (2024) showed how to model thick cylindrical TPE inclusions, by stacking several TPE inclusion disks. The code *EFGRN/EFCMP* has been proposed by Nespoli et al. (2022) to represent TPE inclusion with an arbitrary shape. Nespoli et al. (2023a) proposed the solutions to model cylindrical Thermo-Poro-Visco-Elastic (TPVE) inclusions considering a Maxwell's rheology. In the present article we employ the solutions of Nespoli et al. (2023a) to illustrate the effects on gravity due to a disk-shaped TPE inclusion in a uniform half-space, even we are aware that vertical elastic and density heterogeneities have important effects (e.g. Amoruso et al., 2008). In this work, we focus on the scenario in which temperature and pore pressure increase within the TPE inclusion. Owing to the linear dependence of the induced mechanical fields on Δp and ΔT, opposite variations produce equal and opposite effects; hence, heating-pressurization followed by cooling-depressurization restores the system to its initial state.

2.2. Gravity changes due to a disk-shaped TPE inclusion

The observed gravity change, Δg_{TOT} can be separated into a first term, Δg_{FA} depending on the elevation change (Berrino, 1994) and another additional term, which express the gravity residuals, Δg_R due to mass (i.e. density) redistribution (e.g. Trasatti and Bonafede, 2008; Bonafede and Ferrari, 2009; Sasai, 1986):

$$\Delta g_{TOT} = \Delta g_{FA} + \Delta g_R \tag{6}$$

The term Δg_{FA} can be removed by the free air correction, accounting for the vertical displacement of a ground-based benchmark, and it is computed as $\Delta g_{FA} = u_z 2g/R$, where g is the acceleration of gravity and R is the distance from the Earth's center to the benchmark. At 45° of

latitude, $\Delta g_{FA} = u_z 2g/R = 0.3086 u_z$ mGal. The second term can be expressed as follows:

$$\Delta g_R = G\int_V \Delta\rho \frac{\cos\gamma}{|\ell|^2} dV = \Delta g_L + \Delta g_V + \Delta g_d \quad (7)$$

with

$$\Delta g_L = G\int_V \mathbf{u}\cdot\nabla\rho\frac{\cos\gamma}{|\ell|^2} dV \quad (8)$$

$$\Delta g_V = -G\int_V \rho e_{kk}\frac{\cos\gamma}{|\ell|^2} dV \quad (9)$$

$$\Delta g_d = G\int_V \delta\rho_d\frac{\cos\gamma}{|\ell|^2} dV \quad (10)$$

where V is the total volume embedding non-negligible density variations $\Delta\rho$, with respect to the reference density, ρ, G is the gravitational constant, $\boldsymbol{\ell}$ is the vector between the infinitesimal element dV and the observation point, γ is the angle between $\boldsymbol{\ell}$ and the downward vertical axis z. The term Δg_L is due to the displacement of reference density heterogeneities within V (the most notable being the displacement of the free surface boundary); Δg_V accounts for the density changes due to the compressibility of the rocks, and Δg_d accounts for density changes $\delta\rho_d$ within the TPE source, including the emplacement of new mass from remote distance (Fig. 1).

2.2.1. Computing Δg_L

If we assume that prior to the arrival of new fluids into the TPE inclusion, the density ρ was uniform in the half-space, the term Δg_L computed at the surface $z = 0$ is given simply by the Bouguer correction, so that:

$$\Delta g_L(z=0) = -2\pi G\rho u_z(z=0) \quad (11)$$

(u_z is negative for uplift and positive for subsidence); the density is

$$\rho = \rho_s(1-\phi) + \rho_f\phi \quad (12)$$

with ρ_s and ρ_f the densities of the solid matrix and the fluid, respectively and ϕ the porosity.

2.2.2. Computing Δg_V

The term Δg_V (9) can be computed numerically by generating a fine mesh which discretizes the volume surrounding the TPE inclusion with several cuboids elements (with sizes from 20 to 57 m), marked by an index i, placed at $\mathbf{x}$, with undeformed volume V_i and deformed volume $V_i' = V_i(1 + e_{kk}(\mathbf{x}))$. The term Δg_V in the discretized space can be then expressed as:

$$\Delta g_V \approx -G\rho\sum_{i\notin V_s} e_{kk}^{(i)}\frac{\cos(\gamma_i)}{\ell_i^2}V_i \quad (13)$$

2.2.3. Computing Δg_d

The term Δg_d must be considered as the TPE inclusion is not an empty volume. Such a term derives from the fact that the TPE inclusion changes its volume and its density (accounting for both the solid matrix and the pore fluid compressibility) following changes of pore-pressure and temperature. As we are assuming that the volume of the inclusion increases from V_s to V_s' due to the arrival of new fluid (mass), the term Δg_d can be evaluated as:

$$\Delta g_d = G\int_{V_s'} \rho_d'\frac{\cos\gamma'}{\ell'^2} dV_s' - G\int_{V_s}\rho\frac{\cos\gamma}{\ell^2} dV_s \quad (14)$$

where the deformed configuration is referred with primed variables and the densities inside the TPE inclusion depend on the porosity of the inclusion ϕ. For this purpose, it is convenient to approximate the integrals of Eq. (14) by using (for each cuboid) an expansion in spherical harmonics up to the second order (Bonafede and Mazzanti, 1999) which leads to:

$$\Delta g_d \approx G\sum_{i\in V_s}\left[\left(\frac{\rho_{d(i)}' - \rho}{\ell_i'^2}cos\gamma_i\right)V_i + \left(\frac{\rho_{d(i)}' - \rho}{\ell_i'^2}cos\gamma_i'\right)e_{kk}^{(i)}V_i\right] \quad (15)$$

where the densities for each element of the mesh after deformation can be computed as

$$\rho_{d(i)}' = \frac{[\rho_s(1-\phi) + \rho_f\phi + \Delta m_i]V_i}{V_i'} \quad (16)$$

By considering that the variation in mass content (per unit of undeformed volume) in a TPE medium can be expressed for small variations of porosity ($\Delta\phi$) and fluid density ($\Delta\rho_f$) as $\Delta m = (\rho_f + \Delta\rho_f)(\phi+\Delta\phi) - \rho_f\phi \simeq \rho_f\Delta\phi + \phi\Delta\rho_f$, so that, Δm_i, in each cuboid of the TPE medium (inside the inclusion) can be written as McTigue (1986):

$$\Delta m_i = \rho_f\left[\frac{1}{3H}(\sigma_{kk}^{(i)} + 3\Delta p) - \phi\frac{\Delta p}{K_s'} + \phi\alpha_s\Delta T\right] + \phi\left[\rho_f\frac{\Delta p}{K_f} - \rho_f\alpha_f\Delta T\right] \quad (17)$$

$$= \rho_f\left[\frac{1}{3H}\left(\sigma_{kk}^{(i)} + \frac{3\Delta p}{B}\right) - \phi(\alpha_f - \alpha_s)\Delta T\right] \quad (18)$$

where B is the Skempton's coefficient,

$$B = \frac{1/H}{\phi/K_f + 1/H - \phi/K_s'} \quad (19)$$

The first term in square brackets of Eq. (18) is proportional to the difference between the undrained pore pressure ($-B\sigma_{kk}/3$) and Δp. It accounts for the increase of pore pressure at constant temperature and for the increase in the volume of fluid that may be hosted in the cavities due to fluid compression. The second term arises from the thermal expansion of the cavities within the solid matrix and the thermal increase of the fluid volume filling them. To better understand the contributions to density variations it is convenient to express it considering three different terms as follows:

$$\Delta\rho_{TOT(i)} = \rho_{d(i)}' - \rho = \Delta\rho_{V(i)} + \Delta\rho_{P(i)} + \Delta\rho_{T(i)} \quad (20)$$

where

$$\Delta\rho_{V(i)} = [\rho_s(1-\phi) + \rho_f\phi]\frac{V_i}{V_i'} - \rho, \quad (21)$$

$$\Delta\rho_{P(i)} = \rho_f\left[\frac{1}{3H}\left(\sigma_{kk}^{(i)} + \frac{3\Delta p}{B}\right)\right]\frac{V_i}{V_i'}, \quad (22)$$

$$\Delta\rho_{T(i)} = \rho_f[-\phi(\alpha_f - \alpha_s)\Delta T]\frac{V_i}{V_i'} \quad (23)$$

considering that $\Delta\rho_{V(i)}$, $\Delta\rho_{P(i)}$, $\Delta\rho_{T(i)}$ are primarily due, respectively, to the volume dilation, the pore-pressure change and the temperature change occurring within the inclusion. In this work we focus on the case $\Delta p > 0$ and $\Delta T > 0$. In the long term after the end of the unrest we expect that both p and T will revert to initial values as well as the gravity residuals. The methodology can be also applied to describe processes involving different signs of Δp and ΔT. For instance, an influx of cold and pressurized fluids within a hot, desaturated inclusion can be represented assuming $\Delta T < 0$ and $\Delta p > 0$, which will not be considered further in this paper.

3. Results

3.1. Cases C1 to C4: Liquid vs vapor filled TPE inclusions

We compute the gravity variations considering a disk-shaped TPE inclusion with a radius $a = 2550$ m, width of $b = 500$ m with median plane located at $z = 1825$ m. This geometry is the one inferred by Nespoli et al. (2021) by inverting the geodetic data of the past (1982–1984) unrest phase of Campi Flegrei (Italy), and was therefore chosen because it is a realistic test-case. We considered four different cases: in C1 and C2 we assume that the TPE inclusion is saturated with water substance (liquid), while in cases C3 and C4 the fluid is vapor (Fig. 2 and Tables 1 and 2). Cases C1 and C3 assume that the arrival of the fluid plume leads to increments of pore-pressure and temperature of $\Delta p = 1$ MPa and $\Delta T = 130$ °C, respectively, while in C2 and C4 $\Delta p = 10$ MPa and $\Delta T = 100$ °C. Such values are choosen in order to get the same TPE inclusion potency, $e_0 = 0.0013$ in all the four cases, leading a maximum surface uplift of ≈0.67 m. The mechanical effects of a TPE inclusion with these characteristics are shown in Fig. 3. The choice of considering the same potency in C1 to C4 cases allows us to explore the effects of gravity variations induced by fluids with different properties, given the same uplift generated by the TPE inclusion. The starting density and the thermal expansion coefficient of the fluid were computed according to the properties of H_2O (Table 2). The TPE parameters of Table 1 are assumed to be constant (i.e. they do not depend on p and T). Fig. 2a shows the phase diagram of water (T_f, P_f) superimposed to its density. For each case C1 to C4 the arrows in the graph show the initial ($T = T_f$, $p = P_f$) and the final state ($T = T_f + \Delta T$, $p = P_f + \Delta p$) of the fluid inside the TPE inclusion (Table 2). We will discuss case C5 in the next section. By "initial state," we refer to the condition of the fluid permeating the TPE inclusion before the arrival of the hot, pressurized fluid plume. The "final state" represents the condition the fluid would reach inside the TPE inclusion, assuming uniform increases of pressure (Δp) and temperature (ΔT). In the 4 cases, C1 to C4, the assumed variations do not involve a state change from liquid to vapor. This allows us not to consider phase transitions. In cases C1 and C3 the starting pressure is lower ($P_f = 5 \cdot 10^5$ Pa) than in cases C2 and C4 ($P_f = 5{\cdot}10^6$ Pa). Fig. 2b shows the different contributions (Eqs. (21), 22, 23) to the density variations obtained in the 4 cases. Let us first note that the contributions to the density variations are generally negative or very small. Total density variations obtained in C1 and C2 are similar (≈ −17 kg/m^3). The greater contribution comes from $\Delta\rho_T$ which explains about 65 % of the total variation. This contribution comes basically from the different volumetric expansion of the fluid and the solid matrix following the increase in temperature and indicates that the heating of the TPE inclusion, i.e. the ΔT, has an important role in the calculation of the gravity variations. A significant contribution (30 %), though the second largest, comes from $\Delta\rho_V$ (≈ −5 kg/m^3), which is associated with volume changes in the individual elements comprising the TPE inclusion. These elements undergo expansion, leading to a reduction in their density. The contribution of $\Delta\rho_p$ is very small and provides in all the three cases by no >5 % of the total density variations. In the cases C3 and C4, where the fluid is water vapor, both the contribution $\Delta\rho_p$ and $\Delta\rho_T$ are low and most of the density variations are due to $\Delta\rho_V$. This is due to the fact that the fluid densities are much smaller with respect to the ones in C1 and C2.

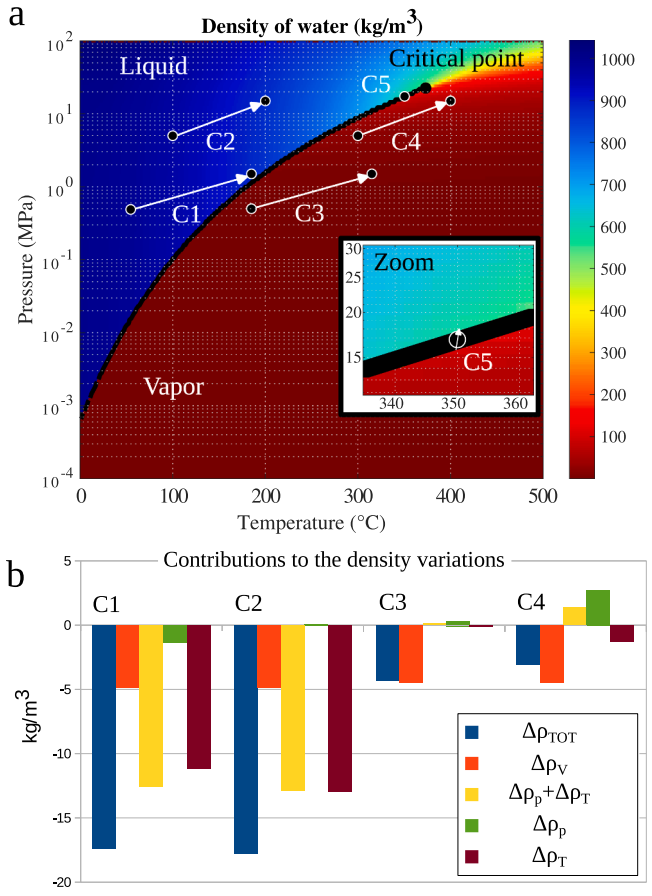

Fig. 2. (a) Fluid densities in cases C1 to C5 (color) plotted in the Clapeyron's phase diagram of water (pressure vs temperature). (b) Different contributions to the density variation computed in the center of the TPE inclusion. The fluid parameters of C1 to C4 are reported in Table 2. The black line is the equilibrium curve.

Table 1
Thermo-Poro-Elastic rock parameters used in the test cases (Nespoli et al., 2021). Subscripts s refer to the solid phase.

Symbol	Parameter	Unit of measure	Value
ρ_s	Density	kg/m^3	2650
ϕ	Porosity	-	0.2
α_s	Thermal expansion	1/K	$3 \cdot 10^{-5}$
μ	Shear modulus	Pa	$6 \cdot 10^9$
λ	Lamè's parameter	Pa	$4 \cdot 10^9$
H	Poroelastic parameter	Pa	$1.01 \cdot 10^{10}$

Fig. 4 shows the gravity variations induced by the TPE inclusions in the four cases. In all cases the Δg_{FA} term deriving from the free air correction is the greatest one in magnitude and reaches about −200 μGal. The negative value is consistent with the fact that for a positive potency the TPE inclusion leads to uplift. Similarly, this is true for the term deriving from the (positive) Bouguer's correction, Δg_L. Δg_V is always negative due to the expansion induced by the inclusion on all the surrounding space, even if it is low in magnitude in all cases (see Fig. 3a and 3b for vertical sections of stress and strain fields). The term Δg_d is larger in absolute value than Δg_V and it is also negative, due to the stronger density decreases, induced by volumetric expansion resulting from positive Δp and ΔT, occurring within the TPE inclusion. The most important value to compare with surface observations is however the residual gravity, Δg_R, which is negative in cases C1 and C2 (reaching about −120 μGal), negligibly small in C3, and positive but small in C4 (≈ 13 μGal).

3.2. Case C5: Discontinuous density changes due to phase changes

A transformation that intersects the equilibrium curve of water (for example, near the critical point, as illustrated in Fig. 2) results in a phase change. In this case, significant density variations can be induced by relatively small and transient changes in pore pressure and/or temperature. Pressure and temperature pulses can be due for example to the arrival (or escape) of a plume of fluids or to rapid fracturing and variations in permeability induced by seismicity and causing changes in the

Table 2
Fluid (subscripts *f*) parameters used in the test cases (https://irc.wisc.edu/properties/ and XSteam (Holmgren, 2025), IAPWS IF-97 standard). P_f and T_f are the assumed initial pressure and temperaure of the fluid, respectively (Fig. 2). In cases C3 and C4, B is computed from the Eq. (19), considering that K_f corresponds to pressure reached in the two cases: 1.5 MPa in C3 and 15 MPa in C4.

Symbol	Parameter	Units	C1-Liquid	C2-Liquid	C3-Vapor	C4-Vapor	C5-L + V
ρ_f	Density	kg/m^3	985.9	960.6	2.440	22.05	102.4
α_f	Thermal expansion	1/K	0.00049	0.00074	0.00250	0.00320	-
B	Skempton parameter	-	0.62	0.62	0.0008	0.008	-
Δp	Pore pressure change	Pa	$1 \cdot 10^6$	$10 \cdot 10^6$	$1 \cdot 10^6$	$10 \cdot 10^6$	0
ΔT	Temperature change	°C	130	100	130	100	0
P_f	Fluid pressure	Pa	$0.5 \cdot 10^6$	$5 \cdot 10^6$	$0.5 \cdot 10^6$	$5 \cdot 10^6$	$17 \cdot 10^6$
T_f	Fluid temperature	°C	55	100	185	300	350

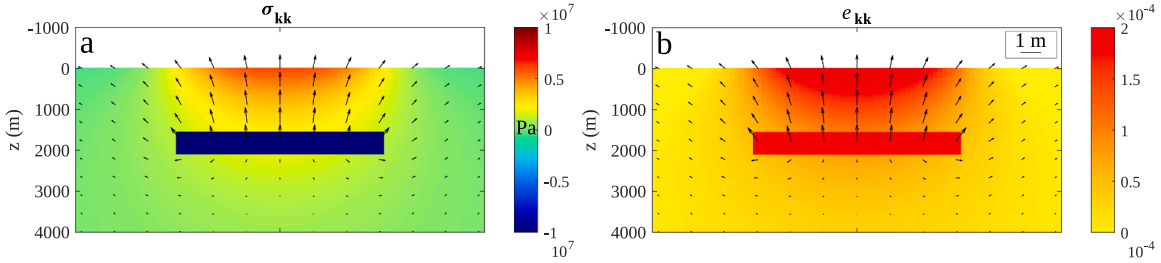

Fig. 3. Vertical sections of the trace of the stress tensor (a) and of the deformation (dilation) (b) for a disk-shaped TPE inclusion with radius $a = 2550$ m, width $b = 500$ m with median plane located at $z = 1825$ m. The TPE inclusion potency is $e_0 = 0.0013$. The assumed TPE parameters are the same as the ones used by Nespoli et al. (2021) and are reported in Table 1. Black arrows represent the displacement.

fluid flow. To account for gravity changes in presence of phase changes we cannot use Eq. (18) as density variations are not small and cannot be computed through K_f and α_f. In this case, Eq. (18) must be rewritten as:

$$\Delta m_i = \rho_f' \left[\frac{1}{3H} \left(\sigma_{kk}^{(i)} + 3\ \Delta p \right) - \phi \frac{\Delta p}{K_s} + \phi \alpha_s \Delta T \right] + \phi\chi \left(\rho_f' - \rho_f \right) \qquad (24)$$

where the finite discontinuity of density, $\Delta\rho_f' = \rho_f' - \rho_f$ is introduced, which reflects the change in fluid density from its initial value, ρ_f, to the final one, ρ'_f, on the other side of the equilibrium curve; χ is the volume fraction of the fluid undergoing phase changes. To study the effects of phase changes, we now analyze how density variations in a thin layer at the top of the inclusion ("transition layer") affect the observed gravity changes. Nearby, the shallow meteoric aquifer (Fig. 1) promotes rapid fluid circulation and consequently a swift redistribution of excess or deficient fluid mass in response to density changes. In the transition layer, the proximity of the cold, shallow meteoric aquifer and the high pressure of the fluids within the TPE inclusion would favor condensation. Conversely, vaporization is favored by the gradual decrease in pressure within the hot, rising plume, which progressively dissipates its overpressure toward the meteoric aquifer. When the fluid is near the equilibrium curve, both liquid and vapor phases coexist. In such conditions, even small fractures or transient fluid flows can quickly alter the balance between gas and liquid saturation within the rock's pores. Case C5 (Inset of Fig. 2a) shows an example of a phase transition occurring during a transformation at constant pressure ($P_f = 17 \cdot 10^6$ Pa, $\Delta p = 0$) and temperature ($T_f = 350$ °C, $\Delta T = 0$) that leads to the condensation of 50 % of the gas ($\chi = 0.5$) and a $\Delta\rho_f \approx 480$ kg/m^3 (Haar et al., 1984). In this case only the last term of the Eq. (24) survives. Case C5 indicates that it is sufficient to consider a transition layer with a thickness of 50 m to obtain positive gravity residuals $\Delta g_R \approx 45$ μGal (i.e. $\Delta g_R \approx 90$ μGal if $\chi = 1$). It is important to note that, in this case, the gravity residuals are calculated assuming a TPE inclusion with $e_0 = 0$. In C5 we focus only on a partial condensation (with $0 < \chi < 1$), as the other terms are irrelevant. In fact, even for reasonable values of the variables (e.g. $\Delta p = 10$ MPa, $\Delta T = 100$ °C, $\phi\chi$ =0.1) the last term of the Eq. (24) is orders of magnitude larger than the others, so $\Delta m_i \approx \phi\chi(\rho'_f - \rho_f)$. This implies that significant gravity variations due to phase changes can occur even for small Δp and ΔT without being linked to significant ground uplift, suggesting that these density variations may produce a large scatter in measured gravity residuals at nearly constant deformation.

3.3. Hints from the Campi Flegrei caldera

The Campi Flegrei caldera in Italy (Fig. 5) has experienced multiple volcanic events over the past 47,000 years. In recent times, its activity has primarily been marked by gas emissions, fumaroles, and rapid ground uplift (bradyseism), followed by periods of ground subsidence (e.g. De Vivo, 2006). A significant uplift occurred between 1982 and 1984, reaching 1.8 m in the city of Pozzuoli (Trasatti et al., 2011). Since 2005, another uplift phase is ongoing, accompanied by increased seismic activity at shallow depth and variations of fumarole emissions (Chiodini et al., 2016). Advancements in geodetic techniques, like InSAR and GNSS, have enabled more precise measurements of smaller uplift episodes in recent years. Despite variations in volcanic activity, the pattern of the surface deformation of the caldera remains stable and nearly symmetrical, centered around Pozzuoli (Nespoli et al., 2023b; Vitale and Natale, 2023). Various models have been used to study the deformation of Campi Flegrei. Most of them are pressurized sources or cracks which are meant to represent volumes of magma (e.g. Amoruso et al., 2008; Trasatti et al., 2011; Bonafede et al., 1986). Bonafede et al. (2022) report a systematic review of them. Nevertheless, models based on hydrothermal circulation also provide a good explanation (e.g. Todesco, 2021; Nespoli et al., 2021), suggesting that the uplift episodes are likely caused by a combination of fluid flow within the shallow hydrothermal system and the emplacement and movement of magma. The current phase of unrest still creates a diversity of interpretations (e.g. Nespoli et al., 2022; Tramelli et al., 2024; Scotto di Uccio et al., 2024; Astort et al., 2024; Giacomuzzi et al., 2025) that, although they favor a constructive scientific debate, suggest that a satisfactory understanding of the phenomenon is not yet close.

Free air corrected gravity residuals measured at the Serapeo location collected between 1980 and 2020 (Berrino and Ricciardi, 2020) are reported in Fig. 5b, while the uplift measured in the city of Pozzuoli by leveling (Del Gaudio et al., 2010) and GNSS (Rione Terra) since 2000 (De Martino et al., 2021) is shown in Fig. 5c. Both locations roughly correspond to the point of greatest ground uplift. Gravimetric data show

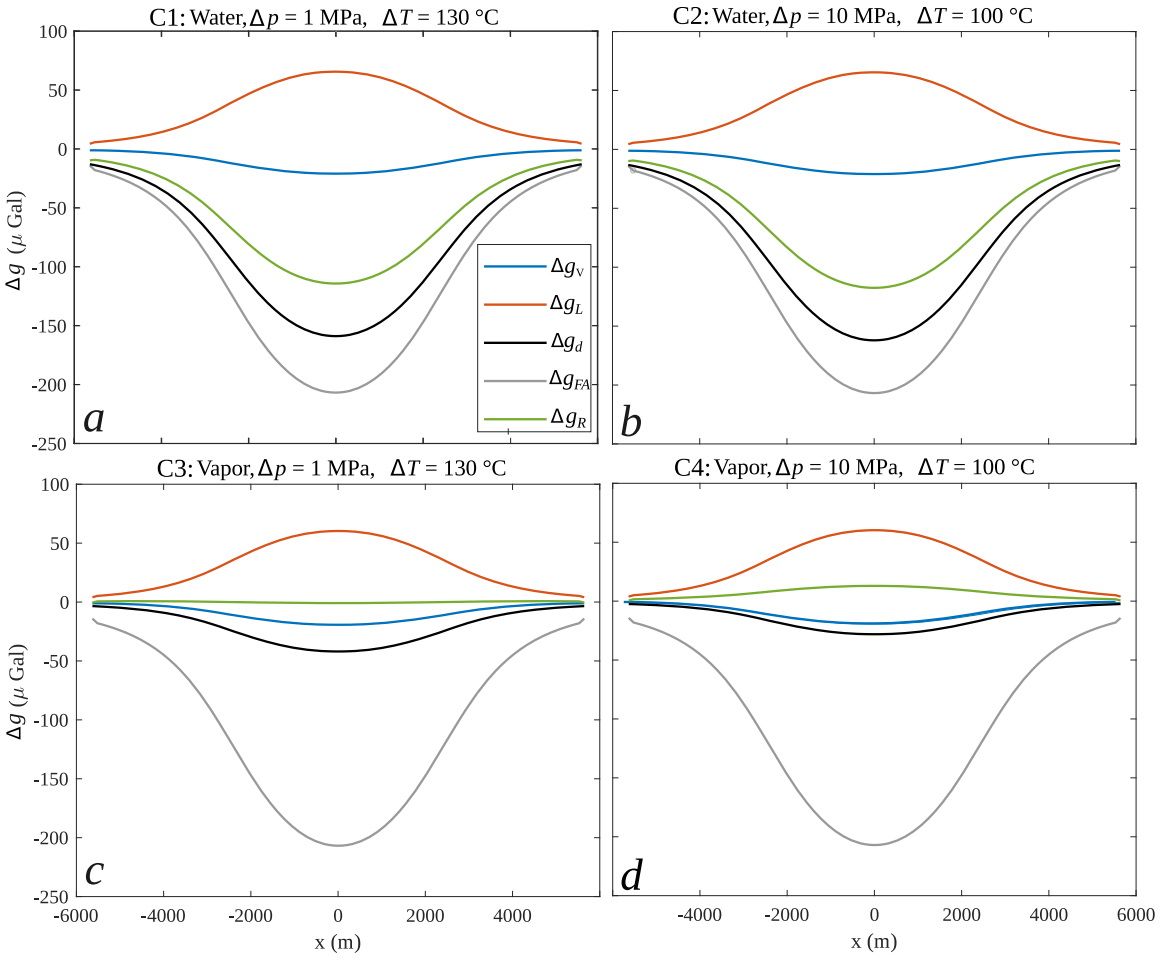

Fig. 4. Gravity changes induced by a disk-shaped TPE inclusion with radius $a = 2550$ m, width $b = 500$ m with median plane located at $z = 1825$ m. Panels a and b are pertinent to TPE inclusions saturated with liquid water substance, while panels c and d the TPE inclusion are vapor saturated. In panels a and c we assumed $\Delta p = 1$ MPa and $\Delta T = 130$ °C, while in panels b and d, $\Delta p = 10$ MPa and $\Delta T = 100$ °C: the TPE inclusion potency is the same in all the panels ($e_o = 0.0013$). The assumed parameters for the solid phase, which are the same as the ones used by Nespoli et al. (2021), as well as the fluid parameters, are reported in Table 1 and Table 2, respectively.

a rapid increase in gravity residuals accompanying the uplift trend during the unrest phase of 1982–1984. The same does not seem to happen in the subsequent unrest phase, since the increase in the uplift detected since 2005 is not accompanied by a net increase of the gravimetric data, which are scattered around values of ± 40 μGal with respect to an average value that has been almost constant since 1990. These oscillations are well above the uncertainty of the data which does not exceed ± 10 μGal (Berrino and Ricciardi, 2020). It is important to remember that the geometrical parameters and the potency, e_0 chosen for the TPE inclusion of section (3.1) were inferred by Nespoli et al. (2021) from the inversion of the geodetic data measured between June 1980 and June 1983. In this period an overall uplift of ≈0.67 m and a gravity residual of ≈45 μGal, were measured respectively at Pozzuoli and Serapeo (Fig. 5). Fig. 5d reports the computed gravity residuals due to the five cases C1 to C5 presented in the previous sections. As we can see, cases C3 and C4 (steam) provide very low residuals that alone cannot explain the increases of gravity observed in the 1982–84 unrest phase. Cases C1 and C2 (liquid water) give rise to strongly negative residuals, which are opposite to those observed in the 1982–84 unrest phase. Case C5 instead explains positive gravity residuals without significant uplift and could explain the oscillations observed after 1985. To compare the TPE inclusions with a magmatic source, we have reported in Fig. 5d the gravity residuals that would be obtained considering a pressurized Mogi's source. We investigated the effects of a Mogi source located beneath the TPE inclusion, with both sources sharing the same vertical symmetry axis. Consistently with Bonafede and Ferrari (2009), we assumed a Mogi source (*M*) located at $d_{(M)}$=3 km, with a radius a_M= 500 m. The overpressure was assumed to be $\Delta P_{(M)}$=362 MPa to realize a maximum uplift equal to 0.67 m. Gravity residuals induced by the Mogi source were computed following Bonafede and Ferrari (2009) as:

$$\Delta g_{R(M)} \approx \frac{G\,\rho_m V_0}{d_{(M)}^2}\left(\frac{\Delta V_{out}}{V_0}+\frac{\Delta P_{(M)}}{K}\right) \tag{25}$$

where the density of the magma is $\rho_m = 2500$ kg/m^3, $V_0 = 4/3\pi(a_M)^3$ is the source volume and the volume variation of the pressurized sphere is $\Delta V_{out} = 3V_0\,\Delta P_{(M)}/4\mu$. As known from past literature (e.g. Trasatti and Bonafede, 2008), the Mogi source can easily explain gravity changes with a magnitude of some tens of μGal. To provide an additional comparison, we also considered a vertical prolate spheroid (Yang et al., 1988) as another source of deformation. The geometry of the spheroid (*S*) is the one retrieved by the inversion of geodetic data by Gottssmann et al. (2006): major semi-axis of 2.2 km, minor semi-axes of 1.4 km placed at a depth of 2.9 km. In this case the pressure required to produce a maximum uplift of 0.67 m (computed with dMODELS, Battaglia et al., 2013) is much lower (about 11 MPa) with respect to the one of the Mogi source. By assuming an input of material producing $\Delta g_{R(S)} = 45$ μGal (Clark et al., 1986) we should infer a density of 2200 kg/m^3 (Fig. 5). As a final test, we examined the combined effects of TPE inclusion and the Mogi source. By leveraging the superposition principle, we determined

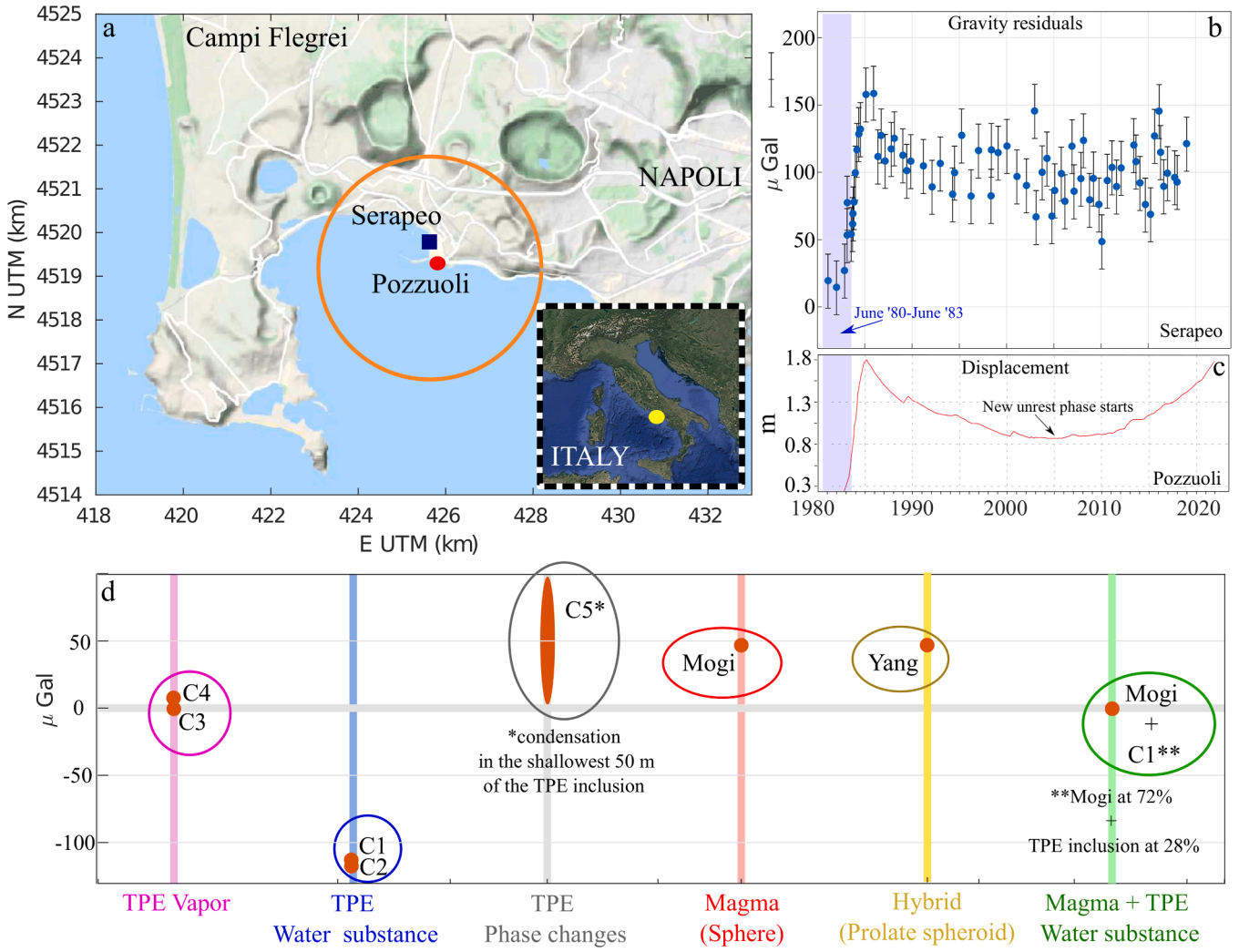

Fig. 5. (a) Map of Campi Flegrei (Italy). The blue square represents the location of measures of gravity residuas (Serapeo); the red circle represents the location of maximum displacement, in the city of Pozzuoli; the orange circle represents the projection of the boundaries of the disk-shaped TPE inclusion inferred by (Nespoli et al., 2021) by inverting the geodetic data in the period June 1980–June 1983. (b) Residuals of gravity (Δg_R) measured at the Serapeo station (Campi Flegrei, Italy) (Berrino and Ricciardi, 2020) from 1980 (blue circles) According to Berrino and Ricciardi (2020), the errors in the gravity data are <10 μGal; however, to account for the errors in the measurements of deformation that may affect the gravity residuals, error bars of ±20 μGal are shown, in agreement with Battaglia et al. (2006). (c) Vertical displacement measured in the city of Pozzuoli (De Martino et al., 2021; Del Gaudio et al., 2010). (d) Computed gravity residuals in cases C1 to C5; due to a Mogi source; due to a Yang source; due to a Mogi source plus a TPE inclusion. All the models in panel d were obtained considering the same elastic parameters of Table 1 and lead to the same maximum uplift (0.67 m). In the latter model the Mogi source accounts for 72 % of the observed uplift (0.48 m), and a shallow TPE inclusion (as in case C1) generates the remaining 28 % (0.19 m).

that the total impact of both sources could be obtained by simply adding their individual contributions to the mechanical fields. This analysis revealed that a system with a deep Mogi source (located at 3 km of depth) accounting for 72 % of the observed uplift, and a shallow liquid filled TPE inclusion (located at 1825 m, as in case C1) contributing the remaining 28 %, would result in zero gravity residuals. This is true regardless of the observed uplift, as the mechanical effects induced by the TPE inclusion and the Mogi source linearly depend on $e_0(\Delta p, \Delta T)$ and $\Delta P_{(M)}$, respectively.

4. Discussion

TPE inclusions play a key role during the unrest phases of volcanic systems since they produce a significant uplift and widespread shallow seismicity without the need to assume the intrusion of magma into the most superficial zones of the volcanic system.

Our results suggest that for the same induced uplift (and thus the same potency) the fluid phase inside the TPE inclusion significantly affects the associated gravity variations (Fig. 5). If the fluid undergoing temperature and pressure changes is liquid water (C1 and C2), the expected gravity residuals at the surface are strongly negative, reaching values as low as −100 μGal in our test cases. In contrast, if the fluid is in a gaseous state (C3 and C4), the resulting gravity variations are minimal or negligible. This suggests that a TPE inclusion can generate substantial uplift without leaving a detectable signature in the residual gravimetric data. This finding highlights the potential for a strong decorrelation between deformation and gravity residuals due to TPE effects. In conventional models, such as pressurized cavities or cracks filled by fluids (e.g., Battaglia et al., 2006), an increase in source volume is usually associated with the addition of new mass, producing positive gravity changes with magnitude depending on the density of the injected material (magma, hydrothermal fluid or hybrid). In contrast, TPE inclusions behave differently: increases in pore pressure and temperature lead to source volume expansion and uplift, but despite this, they can generate decreases in gravity residuals or even produce no detectable gravity variation at all. This occurs because the fluid mass within the

inclusion does not depend solely on its volume, but rather on the combined effects of all TPE parameters that govern the physical behavior of both the solid and fluid phases.

We also found that if the fluid is near the equilibrium curve in the Clapeyron diagram (e.g. Fig. 2), phase changes can induce rapid density variations, producing measurable gravity residuals without significant surface uplift. Such a behavior was observed for example at the Kīlauea Volcano (Hawaii, USA) where the gravity changes without corresponding surface deformation have been attributed to several mechanisms including the replacement of gas-rich magma by denser outgassed magma, magma compressibility, and the filling of void space (Bagnardi et al., 2014). The effect of TPE inclusions represents an additional process that can account for gravity variations in the absence of uplift, emphasizing the role of fluid density changes driven by thermodynamic phase transitions. Accordingly, in the future it will be essential to investigate the nature of the fluid within the inclusion and its specific physical behavior in greater detail. The results of the present work offer only a starting point to continue investigating, which could consider for example fluid mixtures such as H_2O+CO_2, which are generally abundant in volcanic environments (e.g. Chiodini et al., 2021). Considering fluid mixtures instead of pure water can affect the response of a TPE inclusion, as the lower density and higher compressibility of the mixture reduce the gravity signal for a given volume change, while phase separation between liquid and gas can produce rapid local density variations, potentially enhancing the decorrelation between surface uplift and gravity variations. Our results indicate that temperature variations can play an even greater role than pore pressure variations, not only in determining the TPE inclusion potency and thereby the intensity of all mechanical effects (as was already known from Nespoli et al., 2021), but also in influencing gravity variations. In particular, when the fluid inside the inclusion is liquid (C1 and C2), its "high" density makes it more effective in modifying the inclusion's internal density (and thus the resulting gravity variation) in response to thermal expansion of the TPE medium (Fig. 2b).

4.1. Implications for data interpretation

The application of the results to the Campi Flegrei caldera presented in the previous sections allowed us to apply the results to a real case in which the interpretation of data made difficult by the probable coexistence of deformation sources of magmatic and hydrothermal origin. The present work does not aim to resolve the ongoing debate about the cause of the actual unrest at Campi Flegrei. Instead, it seeks to highlight that TPE inclusion models can offer valuable insights in the interpretation of gravimetric data, adding another piece to the puzzle that should not be overlooked. From the application to Campi Flegrei we could understand that it is unlikely that the gravity variations induced by a TPE inclusion alone can explain the residuals observed during the past unrest phase of 1982–1984. In fact, all four case studies C1 to C4 show that TPE inclusions (at least of the geometry considered), cannot provide significant positive gravity variations. This would suggest a significant magmatic contribution during the unrest phase of 1982–1984, as detected by much of the literature (Bonafede et al., 2022, and ref. therein) and the applications of TPE inclusion models (Nespoli et al., 2021). On the other hand, even purely magmatic models have their limitations, because: *i*) several studies based on seismic tomography and deep drillings excluded the presence of large magma bodies (i.e., above the tomographic resolution) in the shallowest kilometers of the caldera (Judenherc and Zollo, 2004; Carlino et al., 2012); *ii*) a single Mogi source cannot fully explain the observed uplift without requiring an overpressure of some hundred MPa: this pressure exceeds the tensile strength of crustal rocks, which is only a few tens of MPa, making it unrealistic for the medium to remain in the elastic regime (Brace and Kohlstedt, 1980). However, this latter issue can be resolved by considering "penny-shaped crack" models and not symmetric sources such as a prolate spheroid which, unlike Mogi's spherical pressurized source models, do not require excessive pressures (e.g. Battaglia et al., 2006; Gottsmann et al., 2006) This is why the combined effect of multiple deformation sources seems to be an unescapable solution.

Through case C5, we estimated the gravitational effects caused by rapid density changes, which can result from phase changes occurring within a thin layer of 50 m containing water near the equilibrium curve of the Clapeyron diagram (P = 17 MPa, T = 350 °C, Fig. 2). This assumption represents a possible scenario in the Campi Flegrei caldera because data from deep wells (Agip, 1987) showed that temperatures up to 420 °C were found at depths <3 km. It is therefore possible that the fluid within the TPE inclusion could be near the critical point of water, (T_c = 374 °C, P_c = 22 MPa). In this scenario, the residual gravity variations are positive, reaching a significant value of approximately 90 μGal when the thin layer completely condensates. However, it is unlikely that these variations alone may account for the 1982–84 unrest, as they are not associated with a significant increase in uplift, contrary to the observations. It is instead likely that they can explain the oscillations (up to ±40 μGal) of the gravity measurements observed in post '82-'84 unrest phase (Fig. 5b) that are not accompanied by significant displacement oscillations. Berrino and Ricciardi (2020), focusing on the period 2015–2019, state that the data generally do not exhibit a clear inverse linear correlation between gravity and height changes. Instead, according to Berrino and Ricciardi (2020), "*a time alternation of gravity decrease/increase has been detected; it suggests an alternation of emptying/replenishment processes*" (driven by shallow fluids). This interpretation is consistent with our results, which indicate that the gravity residuals may be due to cyclical pulses of pore pressure in near-critical fluids (Case C5). A similar interpretation was provided by Gottsmann et al. (2005) for the Nisyros Caldera (Greece), where short-term gravity variations (not correlated with uplift) were attributed to the ascent of steam pockets and transient pressure variations during steam/liquid interface propagation in the shallow hydrothermal system. Anyway, it should be considered that the local gravimetric data could be also influenced by fluid reservoirs that are much smaller than the TPE inclusion but also much shallower.

The application made considering the coexistence of a Mogi source and a TPE inclusion should be considered as a first step for a realistic modeling of the volcanic system in which neither the magmatic nor the hydrothermal contribution is neglected. Such an application is intentionally simplified, since it aims at highlighting the main effect of the superposition of the two sources on gravimetric data. In the future it will be necessary to investigate in more detail the mechanical effects induced by the superposition of the deformation sources. Such an investigation could, for example, implement data inversion approaches that account for the coexistence of multiple sources and consider a layered half-space model, which allows for a more accurate estimate of intrusion densities (e.g., Amoruso et al., 2008); however, this is beyond the scope of the present work.. Nevertheless, even the present simplified analysis shows is that a shallow TPE inclusion, which produces negative gravity residuals, combined with a deeper inflating magma chamber, which causes positive gravity variations, can generate substantial uplift without causing notable gravity residual changes (Case Mogi + C1 in Fig. 5). Moreover, by changing the ratios between the potencies of two sources, we could observe both increases and decreases in gravity residuals, depending on whether the effects of one source prevail over the other. In other words, the TPE inclusion can mask the gravitational effects of magma ascent. Even when the TPE inclusion cannot entirely cancel the gravity effects induced by the magma chamber, it can still significantly reduce them. Recognizing this effect is crucial for avoiding misinterpretations in volcanic hazard assessment, where the absence of gravimetric variations could otherwise be taken as evidence against magmatic intrusions.

The results of the present work can find application to any volcanic system characterized by an active hydrothermal system. For instance, Carbone et al. (2023) suggest that at Mt. Etna the observed gravity decrease may result either from the replacement of dense resident

magma by less dense rising magma or from an increase in exsolved gas in the reservoir, highlighting how the study of the superposition of magmatic and hydrothermal effects can be particularly important. This is the case, for example, at the Long Valley Caldera (Battaglia et al., 1999), the island of Vulcano (Italy) (Stissi et al., 2023), and Cotopaxi volcano (Ecuador), where both types of phenomena can be invoked to explain observed data (Calahorrano-Di Patrea et al., 2019). An interplay between magmatic and hydrothermal processes has been also documented at Te Maari (New Zealand), where the decorrelation between gravity changes and deformation sources was attributed to fluid migration (Miller et al., 2018).

5. Conclusions

The results of this work indicate that the residual gravity variations, due to increases in temperature and pore pressure in a thermo-poro-elastic inclusion are significant. Such variations are strictly related to the phase of the fluid that permeates the inclusion. In our case we have seen that if the fluid inside the inclusion is liquid water the TPE inclusion induces negative gravity residuals, if the fluid is in the gaseous state the TPE inclusion induces very small gravity residuals, while inducing a significant ground uplift. The condensation (or vaporization) of a thin surface layer, on the other hand, would justify large gravity variations that are not associated with significant uplift. The results also show that the heating and pressurization of a TPE inclusion can conceal the gravitational effects of magma ascent. Even when it cannot fully neutralize these effects, it can considerably weaken them. This substantially complicates the interpretation of gravimetric data for hazard assessment, for example in estimating the volumes of magma involved in an unrest phase and emphasizes the need for greater caution when estimating new magma input based solely on geodetic and gravimetric data, without accounting for the influence of the hydrothermal system.

CRediT authorship contribution statement

Massimo Nespoli: Writing – original draft, Visualization, Software, Methodology, Conceptualization. **Maurizio Bonafede:** Writing – review & editing, Methodology. **Maria Elina Belardinelli:** Writing – review & editing, Methodology.

Declaration of competing interest

The authors declare that they have no known competing financial interests or personal relationships that could have appeared to influence the work reported in this paper.

Acknowledgements

The scripts are downloadable here: https://doi.org/10.5281/zenodo.15101527. The authors sincerely thank the editor and reviewers for their valuable comments.

Data availability

https://doi.org/10.5281/zenodo.15101527 (Scripts shared:)

References

Agip, 1987. Geologia e Geofisica del Sistema Geotermico dei Campi Flegrei. Technical report. Servizi Central per l'Esplorazione, SERGMMESG, San Donato.

Amoruso, A., Crescentini, L., Berrino, G., 2008. Simultaneous inversion of deformation and gravity changes in a horizontally layered half-space: evidences for magma intrusion during the 1982–1984 unrest at campi flegrei caldera (italy). Earth Planet Sci. Lett. 272, 181–188.

Astort, A., Trasatti, E., Caricchi, L., Polcari, M., De Martino, P., Acocella, V., Di Vito, M. A., 2024. Tracking the 2007–2023 magma-driven unrest at campi flegrei caldera (italy). Commun. Earth Environ. 5, 506. https://doi.org/10.1038/s43247-024-01665-4.

Bagnardi, M., Poland, M.P., Carbone, D., Baker, S., Battaglia, M., Amelung, F., 2014. Gravity changes and deformation atKīlauea Volcano, Hawaii, associated withsummit eruptive activity, 2009–2012. J. Geophys. Res. Solid Earth 119, 7288–7305. https://doi.org/10.1002/2014JB011506.

Battaglia, M., et al., 1999. Magma intrusion beneath Long Valley Caldera confirmed by temporal changes in gravity. Science 285, 2119–2122. https://doi.org/10.1126/science.285.5436.2119.

Battaglia, M., Segall, P., Roberts, C., 2003. The mechanics of unrest at long valley caldera, california. 2. constraining the nature of the source using geodetic and micro-gravity data. J. Volcanol. Geotherm. Res. 127, 219–245. https://doi.org/10.1016/S0377-0273(03)00171-9.

Battaglia, M., Troise, C., Obrizzo, F., Pingue, F., Natale, G.D., 2006. Evidence for fluid migration as the source of deformation at campi flegrei caldera (italy). Geophys. Res. Lett. 33.

Battaglia, M., Cervelli, P.F., & Murray, J.R. (2013). Modeling crustal deformation near active faults and volcanic centers—A catalog of deformation models and modeling approaches. U.S. Geological Survey Techniques and Methods, book 13, chap. B1, 1–96. https://doi.org/10.3133/tm13B1.

Belardinelli, M., Bonafede, M., Nespoli, M., 2019. Stress heterogeneities and failure mechanisms induced by temperature and pore-pressure increase in volcanic regions. Earth Planet Sci. Lett. 525, 115765. https://doi.org/10.1016/j.epsl.2019.115765.

Belardinelli, M.E., Nespoli, M., Bonafede, M., 2022. Stress changes caused by exsolution of magmatic fluids within an axisymmetric inclusion. Geophys. J. Int. https://doi.org/10.1093/gji/ggac093.

Benussi, C., Belardinelli, M.E., Nespoli, M., 2024. How to model thick thermo-poro-elastic inclusions. Bull. Geophys. Oceanogr. 65, 149. https://doi.org/10.1093/gji/ggw427, 164.

Berrino, G., 1994. Gravity changes induced by height-mass variations at the campi flegrei caldera. J. Volcanol. Geotherm. Res. 61, 293–309. https://doi.org/10.1016/0377-0273(94)90010-8 international Conference on Active Volcanoes and Risk Mitigation.

Berrino, G., Ricciardi, G., 2020. Repeated absolute gravity measurements on a dense network at campi flegrei – a reliable tool for volcano monitoring. Adv. Geosci. 52, 41–54. https://doi.org/10.5194/adgeo-52-41-2020.

Biot, M.A., 1941. General theory of three-dimensional consolidation. J. Appl. Phys. 12, 155–164.

Bonafede, M., Dragoni, M., Quareni, F., 1986. Displacement and stress fields produced by a centre of dilation and by a pressure source in a viscoelastic half-space: application to the study of ground deformation and seismic activity at campi flegrei, italy. Geophys. J. R. Astron. Soc. 87, 455–485. https://doi.org/10.1111/j.1365-246X.1986.tb06632.x.

Bonafede, M., Mazzanti, M., 1999. Residual gravity variations in volcanic areas: constraints to the interpretation of uplift episodes at campi flegrei, italy. Phys. Chem. Earth A: Solid Earth Geod. 24, 963–967. https://doi.org/10.1016/S1464-1895(99)00143-X.

Bonafede, M., Ferrari, C., 2009. Analytical models of deformation and residual gravity changes due to a mogi source in a viscoelastic medium. Tectonophysics 471, 4–13. https://doi.org/10.1016/j.tecto.2008.10.006.

Bonafede, M., Amoruso, A., Crescentini, L., Gottsmann, J.H., Todesco, M., Trasatti, E., 2022. Source Modelling from Ground Deformation and Gravity Changes At the Campi Flegrei Caldera, Italy. Springer Berlin Heidelberg, Berlin, Heidelberg, pp. 283–309. https://doi.org/10.1007/978-3-642-37060111.

Brace, W.F., Kohlstedt, D.L., 1980. Limits on lithospheric stress imposed by laboratory experiments. J. Geophys. Res.: Solid Earth 85, 6248–6252. https://doi.org/10.1029/JB085iB11p06248.

Calahorrano-Di Patre, A., Williams-Jones, G., Battaglia, M., Mothes, P., Gaunt, E., Zurek, J., Ruiz, M., Witter, J., 2019. Hydrothermal fluid migration due to interaction with shallow magma: insights from gravity changes before and after the 2015 eruption of cotopaxi volcano, ecuador. J. Volcanol. Geotherm. Res. 387, 106667. https://doi.org/10.1016/j.jvolgeores.2019.106667.

Calo`, M., Tramelli, A., 2018. Anatomy of the campi flegrei caldera using enhanced seismic tomography models. Sci. Rep. 8. https://doi.org/10.1038/s41598-018-34456-x.

Carbone, D., Cannavò, F., Montagna, C.P., et al., 2023. Gas buffering of magma chamber contraction during persistent explosive activity at Mt. Etna volcano. Commun. Earth Env. 4 (2023), 471. https://doi.org/10.1038/s43247-023-01149-x.

Carlino, S., Somma, R., Troise, C., Natale, G.D., 2012. The geothermal exploration of campanian volcanoes: historical review and future development. Renew. Sustain. Energy Rev. 16, 1004–1030. https://doi.org/10.1016/j.rser.2011.09.023.

Chiodini, G., Caliro, S., Avino, R., Bini, G., Giudicepietro, F., De Cesare, W., Ricciolino, P., Aiuppa, A., Cardellini, C., Petrillo, Z., Selva, J., Siniscalchi, A., Tripaldi, S., 2021. Hydrothermal pressure-temperature control on Co_2 emissions and seismicity at campi flegrei (italy). J. Volcanol. Geotherm. Res. 414, 107245. https://doi.org/10.1016/j.jvolgeores.2021.107245.

Chiodini, G., Paonita, A., Aiuppa, A., Costa, A., Caliro, S., De Martino, P., Acocella, V., Vandemeulebrouck, J., 2016. Magmas near the critical degassing pressure drive volcanic unrest towards a critical state. Nat. Commun. 7, 13712. https://doi.org/10.1038/ncomms13712.

Clark, D.A., Saul, S.J., Emerson, D.W., 1986. Magnetic and gravity anomalies of a triaxial ellipsoid. Explor, Geophys 17, 189–200. https://doi.org/10.1071/eg986189.

Currenti, G., Del Negro, C., Ganci, G., 2007. Modelling of ground deformation and gravity fields using finite element method: an application to etna volcano. Geophys. J. Int. 169, 775–786. https://doi.org/10.1111/j.1365-246X.2007.03380.x.

Currenti, G., Napoli, R., Stissi, S.C., 2024. Thepore: a software package for modeling thermo-poro-elastic displacements. Comput. Geosci. 192, 105716. https://doi.org/10.1016/j.cageo.2024.105716.

D'Auria, L., Massa, B., Cristiano, E., Gaudio, C.D., Giudicepietro, F., Ricciardi, G., Ricco, C., 2014. Retrieving the stress field within the campi flegrei caldera (southern italy) through an integrated geodetical and seismological approach. Pure Appl. Geophys. 172, 3247–3263. https://doi.org/10.1007/s00024-014-1004-7.

Davis, P.M., 1986. Surface deformation due to inflation of an arbitrarily oriented triaxial ellipsoidal cavity in an elastic half-space, with reference to kilauea volcano, hawaii. J. Geophys. Res.: Solid Earth 91, 7429–7438. https://doi.org/10.1029/JB091iB07p07429.

De Martino, P., Dolce, M., Brandi, G., Scarpato, G., Tammaro, U., 2021. The ground deformation history of the neapolitan volcanic area (campi flegrei caldera, somma–vesuvius volcano, and ischia island) from 20 years of continuous gps observations (2000–2019). Remote Sens. (Basel) 13. https://doi.org/10.3390/rs13142725.

De Siena, L., Del Pezzo, E., Bianco, F., 2010. Seismic attenuation imaging of campi flegrei: evidence of gas reservoirs, hydrothermal basins, and feeding systems. J. Geophys. Res.: Solid Earth 115. https://doi.org/10.1029/2009JB006938.

De Vivo, B., 2006. Volcanism in the Campania Plain: Vesuvius, Campi Flegrei and Ignimbrites, 9. Elsevier volume.

Del Gaudio, C., Aquino, I., Ricciardi, G.P., Ricco, C., Scandone, R., 2010. Unrest episodes at campi flegrei: a reconstruction of vertical ground movements during 1905–2009. J. Volcanol. Geotherm. Res. 195, 48–56. https://doi.org/10.1016/j.jvolgeores.2010.05.014.

Eshelby, J.D., 1957. The determination of the elastic field of an ellipsoidal inclusion, and related problems. Proc, R. Soc, L., A 241, 376–396. https://doi.org/10.1098/rspa.1957.0133.

Fernández, J., Rundle, J.B., 1994. Gravity changes and deformation due to a magmatic intrusion in a two-layered crustal model. J. Geophys. Res.: Solid Earth 99, 2737–2746. https://doi.org/10.1029/93JB02449.

Giacomuzzi, G., Fonzetti, R., Govoni, A., De Gori, P., Chiarabba, C., 2025. Causal processes of shallow and deep seismicity at campi flegrei caldera. Commun. Earth Environ. 6, 70. https://doi.org/10.1038/s43247-025-02045-2.

Gottsmann, J., Rymer, H., Wooller, L.K., 2005. On the interpretation of gravity variations in the presence of active hydrothermal systems: insights from the Nisyros Caldera, Greece. Geophys. Res. Lett. 32, L23310. https://doi.org/10.1029/2005GL024061.

Gottsmann, J., Rymer, H., Berrino, G., 2006. Unrest at the Campi Flegrei caldera (Italy): a critical evaluation of source parameters from geodetic data inversion. J. Volcanol. Geotherm. Res. 150, 132–145. https://doi.org/10.1016/j.jvolgeores.2005.07.002.

Gottsmann, J., Komorowski, J.C., Barclay, J., 2019. Volcanic Unrest and Pre-eruptive Processes: A Hazard and Risk Perspective. Springer International Publishing, Cham, pp. 1–21. https://doi.org/10.1007/11157201719.

Haar, L., Gallagher, J.S., Kell, G.S., 1984. NBS/NRC Steam tables: Thermodynamic and Transport Properties and Computer Programs For Vapor and Liquid States of Water in SI Units. Hemisphere, Washington (D.C.). URL. http://lib.ugent.be/catalog/rug01:000139509.

Holmgren, M., 2025. X steam, thermodynamic properties of water and steam. URL. https://it.mathworks.com/matlabcentral/fileexchange/9817-x-steam-thermodynamic-properties-of-water-and-steam.

Judenherc, S., Zollo, A., 2004. The bay of naples (southern italy): constraints on the volcanic structures inferred from a dense seismic survey. J. Geophys. Res.: Solid Earth 109. https://doi.org/10.1029/2003JB002876.

Mantiloni, L., Nespoli, M., Belardinelli, M.E., Bonafede, M., 2020. Deformation and stress in hydrothermal regions: the case of a disk-shaped inclusion in a half-space. J. Volcanol. Geotherm. Res. 403, 107011. https://doi.org/10.1016/j.jvolgeores.2020.107011.

McTigue, D.F., 1986. Thermoelastic response of fluid-saturated porous rock. J. Geophys. Res.: Solid Earth 91, 9533–9542. https://doi.org/10.1029/JB091iB09p09533.

Miller, C.A., Currenti, G., Hamling, I., Williams-Jones, G., 2018. Mass transfer processes in a post eruption hydrothermal system: parameterisation of microgravity changes at Te Maari craters, New Zealand. J. Volcanol. Geotherm. Res. 357, 39–55. https://doi.org/10.1016/j.jvolgeores.2018.04.005.

Mogi, K., 1958. Relations between the eruptions of various volcanoes and the deformations of the ground surfaces around them. Earthq. Res. Inst. 36, 99–134.

Narita, S., Ozawa, T., Aoki, Y., Shimada, M., Furuya, M., Takada, Y., Murakami, M., 2020. Precursory ground deformation of the 2018 phreatic eruption on iwo-yama volcano, revealed by four-dimensional joint analysis of airborne and spaceborne insar. Earth Planets Space 72, 145. https://doi.org/10.1186/s40623-020-01280-5.

Nespoli, M., Belardinelli, M.E., Bonafede, M., 2021. Stress and deformation induced in layered media by cylindrical thermo-poro-elastic sources: an application to campi flegrei (italy). J. Volcanol. Geotherm. Res. 415, 107269. https://doi.org/10.1016/j.jvolgeores.2021.107269.

Nespoli, M., Belardinelli, M.E., Bonafede, M., 2023a. Thermo- poro-viscoelastic response of a disc-shaped inclusion. Geo-Phys. J. Int. 235, 135–149. https://doi.org/10.1093/gji/ggad212.

Nespoli, M., Belardinelli, M.E., Calò, M., Tramelli, A., Bonafede, M., 2022. Deformation induced by distributions of single forces in a layered half-space: efgrn/efcmp. Comput. Geosci. 164, 105136. https://doi.org/10.1016/j.cageo.2022.105136.

Nespoli, M., Tramelli, A., Belardinelli, M.E., Bonafede, M., 2023b. The effects of hot and pressurized fluid flow across a brittle layer on the recent seismicity and deformation in the campi flegrei caldera (italy). J. Volcanol. Geotherm. Res. 443, 107930. https://doi.org/10.1016/j.jvolgeores.2023.107930.

Nespoli, M., Yu, H., Rinaldi, A.P., Harrington, R., Belardinelli, M.E., Martinelli, G., Piombo, A., 2025. Applications and future developments of the (thermos-) poro-elastic theory in geophysics. Earth-Sci. Rev. 260, 104996. https://doi.org/10.1016/j.earscirev.2024.104996.

Nikkhoo, M., Rivalta, E., 2022. Analytical solutions for gravity changes caused by triaxial volumetric sources. Geophys. Res. Lett. 49, e2021GL095442. https://doi.org/10.1029/2021GL095442.

Okada, Y., 1985. Surface deformation due to shear and tensile faults in a half-space. Bull. Seismol. Soc. Am. 75, 1135–1154.

Polcari, M., Borgstrom, S., Del Gaudio, C., De Martino, P., Ricco, C., Siniscalchi, V., Trasatti, E., 2022. Thirty years of volcano geodesy from space at campi flegrei caldera (italy). Sci. Data 9. https://doi.org/10.1038/s41597-022-01849-7.

Sasai, Y.S., 1986. Multiple tension-crack model for dilatancy; surface displacement, gravity and magnetic change. Bull. Earthq. Res. Inst. = Tokyo Daigaku Jishin Kenkyusho Iho 61, 429–473.

Scotto di Uccio, F., Lomax, A., Natale, J., Muzellec, T., Festa, G., Nazeri, S., Convertito, V., Bobbio, A., Strumia, C., Zollo, A., 2024. Delineation and fine-scale structure of fault zones activated during the 2014–2024 unrest at the campi flegrei caldera (southern italy) from high-precision earthquake locations. Geophys. Res. Lett. 51, e2023GL107680. https://doi.org/10.1029/2023GL107680.

Segall, P., 2010. Earthquake and Volcano Deformation. Princeton University Press. https://doi.org/10.1515/9781400833856.

Stissi, S.C., Currenti, G., Cannavo`, F., Napoli, R., 2023. Evidence of poro-elastic inflation at the onset of the 2021 vulcano island (italy) unrest. Front. Earth Sci. 11. https://doi.org/10.3389/feart.2023.1179095.

Todesco, M., 2021. Caldera's breathing: poroelastic ground deformation at campi flegrei (italy). Front. Earth Sci. 9, 691. https://doi.org/10.3389/feart.2021.702665.

Todesco, M., Berrino, G., 2005. Modeling hydrothermal fluid circulation and gravity signals at the phlegraean fields caldera. Earth Planet Sci. Lett. 240, 328–338. https://doi.org/10.1016/j.epsl.2005.09.016.

Tramelli, A., Convertito, V., Godano, C., 2024. b value enlightens different rheological behaviour in campi flegrei caldera. Commun. Earth Environ. 5, 275. https://doi.org/10.1038/s43247-024-01447-y.

Trasatti, E., Bonafede, M., 2008. Gravity changes due to overpressure sources in 3d heterogeneous media: application to campi flegrei caldera. Italy Ann. Geophys. https://doi.org/10.4401/ag-4444.

Trasatti, E., Bonafede, M., Ferrari, C., Giunchi, C., Berrino, G., 2011. On deformation sources in volcanic areas: modeling the campi flegrei (italy) 1982–84 unrest. Earth Planet Sci. Lett. 306, 175–185. https://doi.org/10.1016/j.epsl.2011.03.033.

Vitale, S., Natale, J., 2023. Combined volcano-tectonic processes for the drowning of the roman western coastal settlements at campi flegrei (southern italy). Earth Planets Space 75, 38. https://doi.org/10.1186/s40623-023-01795-7.

Walsh, J.B., Rice, J.R., 1979. Local changes in gravity resulting from deformation. J. Geophys. Res.: Solid Earth 84, 165–170. https://doi.org/10.1029/JB084iB01p00165.

Wong, T.f., Walsh, J.B., 1991. Deformation-induced gravity changes in volcanic regions. Geophys. J. Int. 106, 513–520. https://doi.org/10.1111/j.1365-246X.1991.tb06325.x.

Yang, X.M., Davis, P.M., Dieterich, J.H., 1988. Deformation from inflation of a dipping finite prolate spheroid in an elastic half-space as a model for volcanic stressing. J. Geophys. Res.: Solid Earth 93, 4249–4257. https://doi.org/10.1029/JB093iB05p04249.

Zencher, F., Bonafede, M., Stefansson, R., 2006. Near-lithostatic pore pressure at seismogenic depths: a thermoporoelastic model. Geophys. J. Int. 166, 1318–1334. https://doi.org/10.1111/j.1365-246X.2006.03069.x.